ISSN 2522-9400 **European Modern Studies Journal** *Vol 8 No 5*
available at www.journal-ems.com
DOI: 10.59573/emsj.8(5).2024.18

Non-Isothermal Steady Flow through a Rotating Square Straight Duct with Hall and Ion-Slip Currents

Md. Rafiqul Islam[1]*, Md. Abdus Samad[2] and Md. Mahmud Alam[3]
[1]Department of Mathematics, Bangabandhu Sheikh Mujibur Rahman Science and Technology University, Gopalganj-8100, Bangladesh
[2]Department of Applied Mathematics, University of Dhaka, Dhaka-1000, Bangladesh
[3]Mathematics Discipline, Khulna University, Khulna-9208, Bangladesh

Abstract. This research delved into examining the behavior of fully developed, viscous, non-isothermal, steady, laminar, incompressible fluid flow along the centerline of a straight square duct, considering the influence of magnetic fields as well as Hall and Ion-slip currents. To make the non-isothermal state of the flow, the right hand wall of the duct is considered as heated whereas left hand wall is cooled; the lower and upper walls are considered as adiabatic. A constant pressure gradient force, known as the Dean Force, is exerted along the centerline of the duct. Additionally, external forces, including gravitational force, Lorentz force, pressure gradient force, centrifugal force, and Coriolis force, influence the flow. The Lorentz force is also modified by applying the Hall and Ion-slip currents. The governing equations are derived from the continuity equation, the Navier-Stokes equation, and the energy equation. The spectral method is employed as the primary tool to obtain numerical solutions, complemented by secondary tools such as Chebyshev polynomials, Newton-Raphson method, collocation method, and arc-length method. The study examines the impact of various parameters, including the Grashof number (G_r), Taylor number (T_r), Dean number (D_n), magnetic parameter (M), Hall parameter (m), and Ion-slip parameter (α), on the velocity and temperature distributions within the flow. This investigation is conducted by analyzing solution curves of flux against the mentioned parameters. Furthermore, the corresponding flow patterns are analyzed at different points along the straight duct. As the new findings, the results are shown under the various distinct values of M, m and α at Dean Number D_n=500, 5000, 10000 with Taylor number is fixed at T_r=20.

Keywords: Dean Force, Lorentz force, Coriolis force, Straight duct, Hall and Ion-slip currents

1. Introduction

In an engineering application, the study of fluid flow through a non-isothermal curved duct has the utmost importance. The magnetic systems of rotating mechanisms also have a significant impact in the electromagnetic field. In the presence of a magnetic field, Hall and ion-slip currents also have an impact on the electrically conducting fluid. Regarding fully developed fluid flow in a curved duct, a pile of studies has been conducted throughout the long span of time. The great Mathematician Dean (1927, 1928), a pioneering author, demonstrated how a pair of counter-rotating vortices flow in a curved pipe. The flow of a viscous incompressible fluid under a constant pressure gradient force is dependent on a parameter $D_n = \frac{G\,d^3}{\mu \upsilon}\sqrt{\frac{2d}{L}}$, also known as the Dean Number according to his name. The flow condition within the curved duct is commonly referred to as Dean's hydro-dynamical instability. The additional vortices that manifest within this flow are often termed Dean's vortices. This type of flow is also recognized as Dean Flow.

* Corresponding Author

Throughout the subsequent decades, a substantial body of research was dedicated to the theoretical and experimental exploration of fluid flow through both curved and straight ducts, with some studies incorporating systems featuring rotation. Notable researchers in this field include Berger et al. (1983), Nandakumar and Masliyah (1982, 1986), Winters (1987), Yanase et al. (1989, 2002), Ishigaki (1996), Yamamoto et al. (1999, 2000, 2006), Chandratilleke et al. (2003, 2012, 2013), Wang and Yang (2003, 2004), and numerous others who have contributed significantly to our understanding of fluid flow in ducts. The source provides a concise overview of several studies focused on curved duct flow. In the context of curved pipes, Berger et al. (1983) conducted research on fully developed flow, exploring both stable and unstable conditions. This investigation encompassed different geometries, wall characteristics, fluid properties, and Dean numbers to assess their respective importance in the context of curved duct flow. Nandakumar and Masliyah (1982, 1986) delved into the study of heat-transferable vortex flow within coiled and curved pipes, considering both whirling flow and steady laminar flow in ducts with square cross-sections. Winters (1987) employed a complex structure featuring a multitude of symmetric and asymmetric solutions to explore laminar bifurcation flow in a curved tube characterized by a rectangular cross-section. Ishigaki (1996) delved into the study of flow patterns and frictional forces in small-curvature circular pipes, both in co-rotating and counter-rotating configurations. Selmi et al. (1994, 1999) conducted research to investigate the impact of Coriolis and centrifugal forces on pressure-driven two-dimensional flow within a rotating curved duct featuring a rectangular cross-section. Yanase et al. (1989) quantitatively examined the stability of dual solutions, namely the 2-vortex and 4-vortex solutions, within a slightly curved tube featuring a circular cross-section. This investigation spanned a wide range of Dean Numbers. Yamamoto et al. (1999, 2000) conducted observations of flow within a rotating system, focusing on both a square-curved duct and a circular pipe with a helical cross-section. The flow they investigated was viscous, incompressible, and continuous. Zhang et al. (2001) explored the combined effects of Coriolis and centrifugal forces on isothermal flows. Their study was conducted in a curved duct with a rectangular cross-section that exhibited rotational characteristics. Yanase et al. (2002) delved into the examination of viscous incompressible laminar flow within a rectangular curved duct, covering a wide range of the extended aspect ratio from 1 to 12. Wang and Yang (2003, 2004) carried out a comprehensive examination, combining numerical simulations and experimental investigations, on fully developed free and forced convection flows within a rotating curved duct characterized by a square cross-section.

Yamamoto et al. (2006) employed a visualization technique in their experimental assessment to study the characteristics of secondary flow within a curved pipe featuring a square cross-section. Yanase et al. (2008) conducted a comprehensive analysis of travelling-wave solutions, comparing the spectral approach with the two-dimensional analysis of experimental studies focusing on the flow within a curved square duct. Wang and Liu (2007) embarked on an investigation that delved into the effects of curvature, initial conditions, stability, instability, and the structure of the fully developed bifurcation of forced convection flow. This study was carried out within a curved square duct characterized by a micro-channel and a small curvature ratio of 5E-06. Subsequently, they conducted a numerical investigation of the fully developed forced convection bifurcation structure in a tightly coiling square cross-section duct with a curvature ratio of 0.5, focusing on the high Dean Number region. Norouzi et al. (2009) concentrated on understanding how primary and secondary normal stress differences impacted forced convection heat transfer in the context of viscoelastic fluid flow within curved ducts. Liu and Wang (2009) delved into the physical factors that give rise to variable structure flow within fully developed forced convection curved ducts characterized by a rectangular cross-section. Fellouah et al. (2010) employed both experimental and numerical methods to investigate the influence of fluid rheology on Dean instability in power-law and

Bingham fluids. They conducted these studies within a curved rectangular duct. Chandratilleke et al. (2003, 2012, 2013) explored laminar flow behaviour and related thermal factors to understand the formation of secondary vortices within fluid flow along curved passageways. Their research also included examinations of the results of secondary flow experiments conducted under different aspect ratios. Wu et al. (2013) used the spectral method to examine the secondary flow of streamlines within a curved square duct. Kun et al. (2014) employed ultrasonic Doppler velocimetry and microphones to investigate both laminar and turbulent flows of pseudo-plastic fluids within a curved square duct characterized by significant curvature. Razavi et al. (2015) conducted research in a rotating curved duct featuring a square cross-section. They explored the effects of the force ratio, Dean Number, and dimensionless heat flux at the wall on the generation of entropy. This was achieved by applying the second law analysis to forced convection laminar flow. Li et al. (2016) explored fully developed three-dimensional flow, both numerically and physically, within a curved rectangular duct. This duct featured a configuration with spiral, double circular, and involutes line curvatures.

In addition, the researchers briefly examined the influence of Reynolds number, aspect ratio, and various curvatures on Dean Instability. This investigation aimed to precisely identify the centre of the secondary base vortices. In a separate study, Li et al. (2017) conducted a numerical investigation of pressure-driven, fully developed turbulent viscous incompressible fluid flow within curved rectangular ducts. It's worth noting that, to the best of our knowledge, no research on non-isothermal magneto-hydrodynamic (MHD) fluid flow in curved ducts with Hall and ion-slip currents has been identified in available sources online. Given that much of the universe consists of highly charged particles and is enveloped by a magnetic field, the innovative concept of incorporating Hall and ion-slip currents into MHD flow within a rotating curved duct in the presence of a magnetic field holds significant importance and potential applications in various engineering and industrial processes.

As a result, the goal is to examine the flow behaviour of non-isothermal steady flow through a rotating square straight duct with hall and ion-slip currents. The numerical solution is computed by using the spectral approach as the primary tool, and the Chebyshev polynomial, Collocation method, and Newton-Raphson method as supplemental tools. Any point in the crucial zone on the solution curve has been calculated using the arc-length method.

2. Mathematical Formulations

The vector form of the governing equations is represented as follows:

Equation of Continuity:

$$\nabla.\mathbf{q}=0 \tag{1}$$

Equation of Momentum:

$$\frac{\partial \mathbf{q}}{\partial t}+(\mathbf{q}.\nabla)\mathbf{q}=\mathbf{F}-\frac{1}{\rho}\nabla p-\upsilon\,\nabla^2\mathbf{q}+\frac{1}{\rho}(\mathbf{J}\wedge\mathbf{B})-2(\Omega\wedge\mathbf{q})+\beta\mathbf{g}T \tag{2}$$

Equation of Energy:

$$\frac{\partial T}{\partial t}+(\mathbf{q}\cdot\nabla)T=\frac{k}{\rho C_p}\nabla^2 T \tag{3}$$

Ohm's Law: $\mathbf{J}=\sigma[\mathbf{E}+\mathbf{q}\wedge\mathbf{B}]$ (4)

Consider a thermally fully developed, viscous, incompressible, two-dimensional, MHD fluid flow through a curved duct of height $2h$ and width $2d$, which is rotated with an angular velocity Ω around its vertical y-axis and x, z -axes are perpendicular to it. It is assumed that the inner wall of the duct is cooled and the outer wall is heated so that the duct flow becomes to be a non-isothermal state. The outer wall temperature is taken as $T_0+\Delta T$ and the inner wall is T_0-ΔT where ΔT >0. A pressure gradient force $G = -\frac{\partial p}{\partial z}$ has been applied as an external force along the centreline direction of the duct.

Since electrically conducting fluids are affected by Hall and Ion-slip currents, Ohm's law is generalized as such:

$$\mathbf{J} = \sigma\mu_e(\mathbf{q} \wedge \mathbf{B}) - \frac{m}{B_0}(\mathbf{J} \wedge \mathbf{B}) + \frac{m\alpha}{B_0^2}(\mathbf{J} \wedge \mathbf{B}) \wedge \mathbf{B} \quad (5)$$

Here, $\omega_e \tau_e = m$ where ω_e, τ_e are cyclotron frequency and electron collision time.

The Lorentz force arises from the interaction of the electric field and the magnetic field. This Lorentz force is further influenced and modified by the presence of Hall and ion-slip currents. Consequently, the flow within the duct experiences the combined effects of the pressure gradient force and the Lorentz force. Additionally, the flow is accelerated due to the collective influence of the Coriolis forces and Centrifugal forces. These forces are a result of the system's rotation and the curvature of the duct. Simultaneously, a gravitational force, denoted as $\mathbf{g}$ =(0, g, 0), acts on the fluid flow within the duct, contributing to the overall dynamics of the system. Figure 1 illustrates the coordinate system along with the relevant notation.

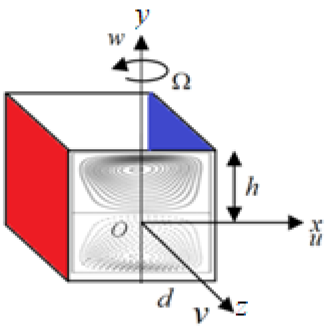

Figure 1: Geometrical model of the present straight square duct

It is also assumed that the body force is absent and all the variables are independent of z except p due to the fully developed flow. Under the above assumptions, the modified governing equation for incompressible fluid is

Equation of Continuity:

$$\frac{\partial u}{\partial x} + \frac{\partial v}{\partial y} = 0 \quad (6a)$$

Equation of Momentum:

$$\frac{\partial u}{\partial t} + u\frac{\partial u}{\partial x} + v\frac{\partial u}{\partial y} = -\frac{1}{\rho}\frac{\partial p}{\partial x} + \upsilon\left(\frac{\partial^2 u}{\partial x^2} + \frac{\partial^2 u}{\partial y^2}\right) + 2\Omega_0 w + \frac{\sigma\mu_e B_0^2}{\rho}\left[\frac{mw - (1+m\alpha)u}{(1+m\alpha)^2 + m^2}\right] \quad (6b)$$

$$\frac{\partial v}{\partial t} + u\frac{\partial v}{\partial x} + v\frac{\partial v}{\partial y} = -\frac{1}{\rho}\frac{\partial p}{\partial y} + \upsilon\left(\frac{\partial^2 v}{\partial x^2} + \frac{\partial^2 v}{\partial y^2}\right) + \beta g T \quad (6c)$$

$$\frac{\partial w}{\partial t} + u\frac{\partial w}{\partial x} + v\frac{\partial w}{\partial y} = -\frac{1}{\rho}\frac{\partial p}{\partial z} + \upsilon\left(\frac{\partial^2 w}{\partial x^2} + \frac{\partial^2 w}{\partial y^2}\right) - 2\Omega_0 u - \frac{\sigma\mu_e B_0^2}{\rho}\left[\frac{mu + (1+m\alpha)w}{(1+m\alpha)^2 + m^2}\right] \quad (6d)$$

Equation of Energy:

$$\frac{\partial T}{\partial t}+u\frac{\partial T}{\partial x}+v\frac{\partial T}{\partial y}=\frac{k}{\rho C_p}\left(\frac{\partial^2 T}{\partial x^2}+\frac{\partial^2 T}{\partial y^2}\right) \tag{6e}$$

2.1 Non-Dimensional Analysis

To make dimensionless form of the governing equations (6a)-(6e), use respective length d and the kinematic viscosity υ, the non-dimensional uniform velocity is defined by $U_0=\upsilon/d$. And it has been introduced some dimensionless quantities

$$x'=\frac{x}{d}\quad \bar{y}=\frac{y}{d};\quad z'=\frac{z}{d};\quad u'=\frac{d}{\upsilon}u;\quad v'=\frac{d}{\upsilon}v;$$

$$w'=\frac{d}{\upsilon}w;\quad t'=\frac{\upsilon}{d^2}t;\quad p'=\frac{d^2}{\rho\upsilon^2}p;\quad \text{and}\quad T'=\frac{T}{\Delta T}$$

where $x', \bar{y}$ and z' are the non-dimensional horizontal, vertical and axial coordinates respectively; u', v', w' are the non-dimensional velocity components in the direction of $x', \bar{y}$ and z' respectively; t' is the non-dimensional time; T' is the non-dimensional temperature and p' is also the dimensionless pressure. By putting these terms into the equations (6a)-(6e) and dropping the primes on the variables, it can be written the above governing equations into its non-dimensional form as follows:

Equation of Continuity

$$\frac{\partial u}{\partial x}+\frac{\partial v}{\partial \bar{y}}=0 \tag{7a}$$

Equation of Momentum

$$\frac{\partial u}{\partial t}+u\frac{\partial u}{\partial x}+v\frac{\partial u}{\partial \bar{y}}=-\frac{\partial p}{\partial x}+\left(\frac{\partial^2 u}{\partial x^2}+\frac{\partial^2 u}{\partial \bar{y}^2}\right)+T_r\,w+\frac{M}{(1+m\alpha)^2+m^2}\big(mw-(1+m\alpha)u\big) \tag{7b}$$

$$\frac{\partial v}{\partial t}+u\frac{\partial v}{\partial x}+v\frac{\partial v}{\partial \bar{y}}=-\frac{\partial p}{\partial \bar{y}}+\left(\frac{\partial^2 v}{\partial x^2}+\frac{\partial^2 v}{\partial \bar{y}^2}\right)+G_rT \tag{7c}$$

$$\frac{\partial w}{\partial t}+u\frac{\partial w}{\partial x}+v\frac{\partial w}{\partial \bar{y}}=D_n+\left(\frac{\partial^2 w}{\partial x^2}+\frac{\partial^2 w}{\partial \bar{y}^2}\right)-T_ru-\frac{M}{(1+m\alpha)^2+m^2}\left[mu+(1+m\alpha)w\right] \tag{7d}$$

Equation of Energy:

$$\frac{\partial T}{\partial t}+u\frac{\partial T}{\partial x}+v\frac{\partial T}{\partial \bar{y}}=\frac{1}{P_r}\left(\frac{\partial^2 T}{\partial x^2}+\frac{\partial^2 T}{\partial \bar{y}^2}\right) \tag{7e}$$

Now let us consider the stream function $u=\frac{\partial\psi}{\partial\bar{y}}$ and $v=-\frac{\partial\psi}{\partial x}$, These are the secondary velocity in terms of stream function ψ which satisfies the continuity equation (7a). Therefore these can be used into the other equations of the governing equations. and also using another transformation $\tilde{y}=hy$ which gives a unique variable y such that $\bar{y}=ly$, where $l=h/d$ is the aspect ratio of the duct.

Finally the central line (axial) direction of equation of Momentum

$$D_n+\frac{\partial^2 w}{\partial x^2}+\frac{1}{l^2}\frac{\partial^2 w}{\partial y^2}+\frac{1}{l}\left(\frac{\partial\psi}{\partial x}\frac{\partial w}{\partial y}-\frac{\partial\psi}{\partial y}\frac{\partial w}{\partial x}\right)-\frac{T_r}{l}\frac{\partial\psi}{\partial y}-\frac{M}{(1+m\alpha)^2+m^2}\frac{1}{l}m\frac{\partial\psi}{\partial y}-\frac{M(1+m\alpha)}{(1+m\alpha)^2+m^2}w=0 \tag{8a}$$

Stream line for the secondary velocity of equation of Momentum

$$\left(\frac{\partial^4\psi}{\partial x^4}+\frac{2}{l^2}\frac{\partial^4\psi}{\partial x^2\partial y^2}+\frac{1}{l^4}\frac{\partial^4\psi}{\partial y^4}\right)-\frac{1}{l}\left(\frac{\partial^3\psi}{\partial x^3}+\frac{1}{l^2}\frac{\partial^3\psi}{\partial x\partial y^2}\right)\frac{\partial\psi}{\partial y}+\frac{1}{l}\left(\frac{\partial^3\psi}{\partial y\,\partial x^2}-\frac{1}{l^2}\frac{\partial^3\psi}{\partial y^3}\right)\frac{\partial\psi}{\partial x}$$

$$+\frac{T_r}{l}\frac{\partial w}{\partial y}+\frac{M}{(1+m\alpha)^2+m^2}\frac{1}{l}\,m\frac{\partial w}{\partial y}-\frac{M(1+m\alpha)}{(1+m\alpha)^2+m^2}\frac{1}{l^2}\frac{\partial^2\psi}{\partial y^2}-G_r\frac{\partial T}{\partial x}=0 \qquad (8b)$$

And the equation of Energy:

$$\frac{1}{P_r}\left(\frac{\partial^2 T}{\partial x^2}+\frac{1}{l^2}\frac{\partial^2 T}{\partial \bar{y}^2}\right)-\frac{1}{l}\left(\frac{\partial\psi}{\partial y}\frac{\partial T}{\partial x}-\frac{\partial\psi}{\partial x}\frac{\partial T}{\partial y}\right)=0 \qquad (8c)$$

The boundary conditions are as follows :

$$w(\pm1,\bar{y})=w(x,\pm1)=\psi(\pm1,\bar{y})=0$$

$$\left(\frac{\partial\psi}{\partial x}\right)(\pm1,\bar{y})=\psi(x,\pm1)=\left(\frac{\partial\psi}{\partial\bar{y}}\right)(x,\pm1)=0 \qquad (8d)$$

and temperature T at the wall is considered constant

$$T(1,y)=1\,,\quad T(-1,y)=-1\,,\quad T(x,\pm1)=x \qquad (8e)$$

- 2.2 Flux and Mean axial velocity

The flux $\tilde{Q}$ through the duct is defined by $\tilde{Q}=\int_{-h}^{h}\int_{-d}^{d}\tilde{w}\,d\tilde{x}\,d\tilde{y}=vd\,Q$

where, $Q=\int_{-1}^{1}\int_{-1}^{1}w\,dx\,dy$ is the dimensionless total flux.

The mean axial velocity is defined by $\bar{\tilde{w}}=\dfrac{v}{4hd}Q$

3. Numerical Approximations

Gottlieb and Orszag (1977) devised the spectral method for discovering the numerical solution to this problem. This approach has served as the primary tool for determining the numerical solution of equations 8(a)-(e). In this method, the variables $w(x,y)$, $\Psi(x,y)$ and $T(x,y)$ are expanded in a series of expansion functions $\Phi_n(x)$ and $\Psi_n(x)$ consisting of Chebyshev polynomials, which are defined as follows

$$\left.\begin{aligned} w(x,y)&=\sum_{m=0}^{\bar{M}}\sum_{n=0}^{\bar{N}}w_{mn}\Phi_m(x)\Phi_n(y)\\ \Psi(x,y)&=\sum_{m=0}^{\bar{M}}\sum_{n=0}^{\bar{N}}\Psi_{mn}\Psi_m(x)\Psi_n(y)\\ T(x,y)&=\sum_{m=0}^{\bar{M}}\sum_{n=0}^{\bar{N}}T_{mn}\Phi_m(x)\Phi_n(y)+x \end{aligned}\right\} \qquad (9)$$

These expansion functions $\Phi_n(x)$ and $\Psi_n(x)$ are defined as follows:

$$\left.\begin{aligned}\Phi_n(x)&=(1-x^2)C_n(x)\\ \Psi_n(x)&=(1-x^2)^2C_n(x)\end{aligned}\right\} \qquad (10)$$

where, $C_n(x)=\cos(n\cos^{-1}x)$ is the nth order Chebyshev polynomial. $\bar{M}$ and $\bar{N}$ are the truncation numbers in the directions of x and y respectively. The expansion coefficients w_{mn}, ψ_{mn} and T_{mn} are then substituted into the basic equations 8(a)-(e) and the collocation method is applied. As a result, it has been obtained the nonlinear algebraic equations in terms of the coefficients w_{mn}, ψ_{mn} and T_{mn}. The collocation points (x_i, y_i) are defined as follows:

$$x_i = \cos\left\{\pi\left(1-\frac{i}{\overline{\mathrm{M}}+2}\right)\right\}, \quad i=1, \ldots\ldots, \overline{\mathrm{M}}+1$$
$$y_i = \cos\left\{\pi\left(1-\frac{i}{\overline{\mathrm{N}}+2}\right)\right\}, \quad i=1, \ldots\ldots, \overline{\mathrm{N}}+1 \tag{11}$$

These points have been employed to discretize the cross-section of the duct.

The steady solutions are acquired through the Newton-Raphson iteration method. Additionally, the arc-length method is employed to overcome the difficulties near the inflection point in steady solutions. The arc-length equation is

$$\sum_{m=0}^{\overline{\mathrm{M}}}\sum_{n=0}^{\overline{\mathrm{N}}}\left[\left(\frac{dw_{mn}}{ds}\right)^2+\left(\frac{d\psi_{mn}}{ds}\right)^2+\left(\frac{dT_{mn}}{ds}\right)^2\right]=1 \tag{12}$$

The initial approximation of the equations is denoted as $s+\Delta s$ originating from point s in the following manner:

$$\left.\begin{aligned} w_{mn}(s+\Delta s) &= w_{mn}(s)+\frac{dw_{mn}}{ds}\Delta s \\ \psi_{mn}(s+\Delta s) &= \psi_{mn}(s)+\frac{d\psi_{mn}}{ds}\Delta s \\ T_{mn}(s+\Delta s) &= T_{mn}(s)+\frac{dT_{mn}}{ds}\Delta s \end{aligned}\right\} \tag{13}$$

Convergence is ensured by introducing $\varepsilon_\tau < 10^{-8}$, where the subscript τ denotes the iteration number, and ε_τ is defined as:

$$\varepsilon_\tau = \sum_{m=0}^{\overline{\mathrm{M}}}\sum_{n=0}^{\overline{\mathrm{N}}}\left[\left(w_{mn}^{\tau+1}-w_{mn}^{\tau}\right)^2+\left(\psi_{mn}^{\tau+1}-\psi_{mn}^{p}\right)^2+\left(T_{mn}^{\tau+1}-T_{mn}^{\tau}\right)^2\right] \tag{14}$$

Due to the consideration of square duct cross-section the aspect ratio of this duct has been taken $l = h/d = 1$.

3.1 Nusselt Number (Nu)

The Nusselt number (Nu) represents the ratio of convective to conductive heat transfer across the duct. In the steady-state case of the problem, Nu is calculated by:

$$Nu = -\frac{d}{\Delta T}\left\langle \left.\frac{\partial T}{\partial x}\right|_{x=0}\right\rangle \tag{15}$$

Here, $\langle\ \rangle$ denotes the mean of heat transfer from the fluid to the duct walls; d represents the distance between the walls, and ΔT signifies the temperature difference. To compute the heat transfer between the cooled and heated walls, we need to determine the Nusselt numbers for the cool wall Nu_c and the heat wall Nu_h in the steady solution. These are respectively defined as $Nu_c = -\frac{1}{2}\int_{-1}^{1}\left\langle \left.\frac{\partial T}{\partial x}\right|_{x=-1}\right\rangle dy$ and $Nu_h = -\frac{1}{2}\int_{-1}^{1}\left\langle \left.\frac{\partial T}{\partial x}\right|_{x=1}\right\rangle dy$.

3.2 Grid Spaces Accuracy

Prior to execute the FORTRAN program; it is necessary to discuss about grid space accuracy. To achieve reasonable accuracy, it is required to select the equal values for $\overline{\mathrm{M}}$ and $\overline{\mathrm{N}}$, because of the duct's square cross-section. The flux Q has been calculated for several pairs of truncation numbers ($\overline{\mathrm{M}}$, $\overline{\mathrm{N}}$) such as (16, 16), (18, 18), (20, 20) and (22,22). These are displayed in Table 1.

Table 1: Fluxes Q at several pairs of truncation numbers $\overline{\mathrm{M}}$ and $\overline{\mathrm{N}}$ for the fixed values of $T_r = 20,\ D_n = 500,\ P_r = 7,\ M = 0,\ m = 0,$ and $\alpha = 0$

$\overline{\mathrm{M}}$	$\overline{\mathrm{N}}$	Q
16	16	221.0305027708467
18	18	221.0309667187638
20	20	221.0309062038524
22	22	221.0308693799025

This table shows that the numerical results are sufficient accurate at ($\overline{\mathrm{M}}$, $\overline{\mathrm{N}}$)=(20, 20).

4. Results and Discussion

The study initially focused on understanding the impact of Grashof number (G_r), Taylor number (T_r), and Dean Number (D_n) on flow patterns under the following fixed conditions: magnetic parameter (M = 0), Hall parameter (m = 0), and Ion-slip parameter (α = 0). This investigation allowed for a deeper understanding of the inherent flow characteristics.

Following this initial analysis, a subsequent investigation explored the influence of additional parameters: the magnetic parameter, Hall parameter, and the Ion-slip parameter, on fluid flow. These results were presented in a solution curve, along with corresponding flow structures. The simulations were conducted under fixed values of the Prandtl number Pr = 7 and Taylor number Tr = 20, with three different Dean Numbers D_n = 500, 5000, and 10000. The program employed increments Δw=50, $\Delta\psi$=0.5 and ΔT=0.1to execute these analyses.

4.1 Effects of Grashof Number (G_r) on the Fluid Velocity and Temperature

In Figure 2a, the solution curve illustrates the relationship between the Grashof Number (G_r) and (i) velocity flux and (ii) mean Nusselt number, representing temperature variations with respect to the Grashof number, at the cooling and heating walls. These results are presented with fixed values of D_n = 500, P_r = 7, M = 0, m = 0 and α = 0.

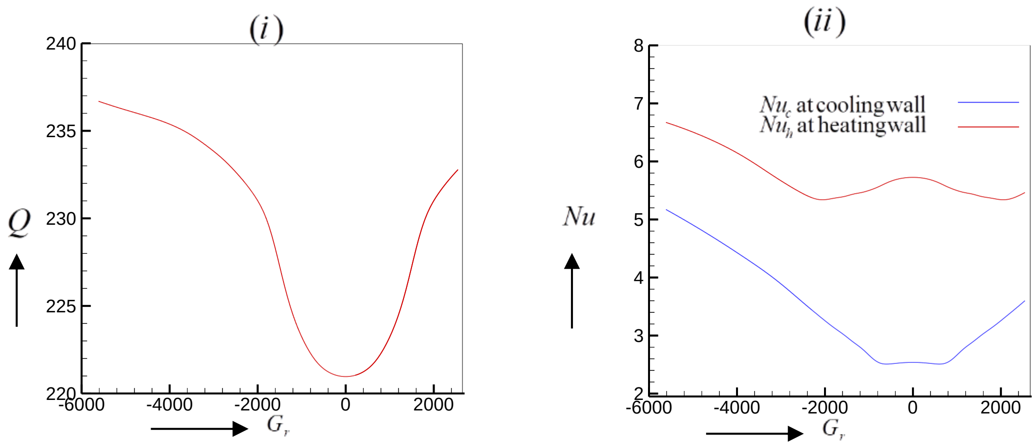

Figure 2a: Solution curve of G_r versus (i) flux Q (ii) Mean Nusselt number Nu at the heating and cooling wall for fixed D_n = 500, T_r = 20, P_r = 7, M = 0, m = 0 and α=0.

For the flux, a single branch of a symmetric solution curve is evident, bounded within the range $G_r \leq 2547$. This curve demonstrates that the flux increases for positive G_r values but decreases for negative G_r values. Regarding temperature, it's noteworthy that the Nusselt number values at the heating wall consistently exceed those at the cooling wall. Additionally, the temperature deviation gradually decreases, albeit at a slow rate, as the absolute value of $|G_r|$ increases.

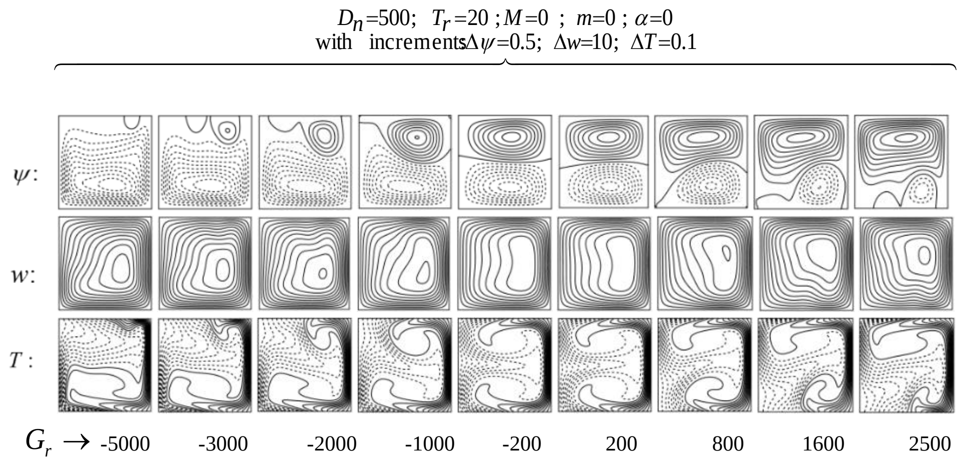

Figure 2*b*: Streamlines ψ (top), axial Contour flow w (middle) and Temperature profile T (bottom) in accordance with the solution curve in Fig.2*a*.

In Figure 2*b*, corresponding flow and temperature structures at various points are depicted. Two vortex asymmetric flows have been identified in the secondary flow. Meanwhile, in the axial flow, a simple contour is evident. The solution structure is notably influenced by the increase in the Grashof number. As the Grashof number increases, the asymmetric structures gradually become more prominent in both positive and negative directions. This asymmetry is primarily attributed to the influence of gravity. With the increase in rotation, the Coriolis force is counterbalanced by the Centrifugal force, pressure gradient force, and Lorentz force. This equilibrium results in the flow structure becoming approximately symmetric. However, the gravitational force acting on the fluid flow as an additional force introduces asymmetry into the flow pattern.

4.2 Effects of Taylor Number (T_r) on the Fluid Velocity and Temperature

Figure 3*a* presents the solution curve of Taylor Number (T_r) versus (*i*) velocity flux (Q) and (*ii*) mean Nusselt number (Nu), which represents temperature variations, at the cooling and heating walls. These results are obtained with fixed values of D_n=1000, G_r=200, P_r=7, M=0, m=0, and α=0 Figure 3*b* displays the corresponding flow structures at various points of Tr on these solution curves for velocity and temperature distribution. As | T_r | increases, the strength of the secondary flow pattern becomes more pronounced, while the axial flow weakens. A critical zone is reached when the Taylor number reaches | T_r |=672. When T_r >0, an increase in T_r results in the dominance of positive directed flow at the top of the duct, with it prevailing over the negative directed flow in terms of streamlines. However, the center of the axial flow contour gradually shifts closer to the cooling wall of the duct. In terms of temperature, the heating fluid dominates over the cooling fluid. Conversely, when T_r <0, the opposite effect occurs as compared to T_r >0.

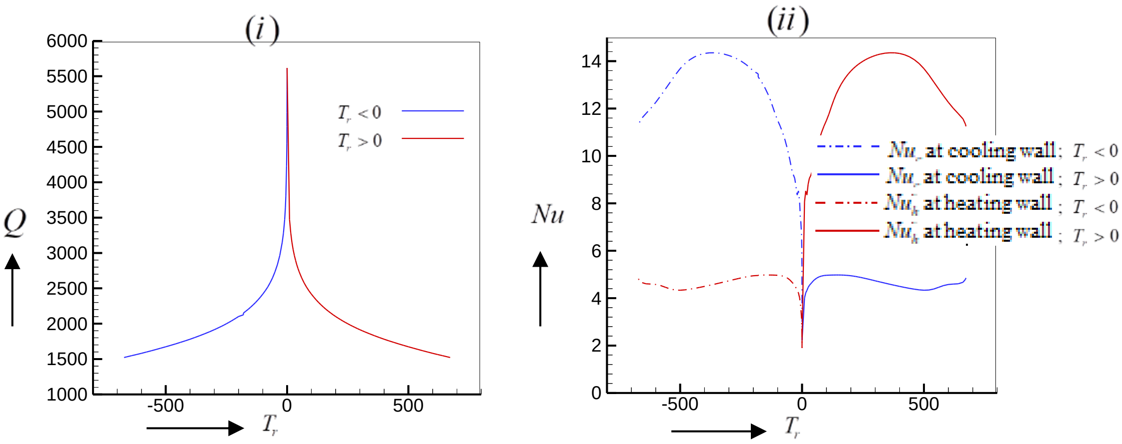

Figure 3*a*: Solution curve of T_r versus (*i*) flux Q (*ii*) Mean Nusselt number Nu at the heating and cooling wall for fixed D_n = 10000, G_r = 200, P_r = 7, M = 0, m = 0 and α=0.

The solution curve is bound within the range -672≤ T_r ≤672 and is symmetric about the vertical line at T_r=0. For the flux, it decreases for positive T_r but increases for negative T_r. In terms of temperature, for positive T_r, the Nusselt number values at the heating wall are greater than those at the cooling wall, while the opposite holds true for negative T_r. No temperature deviation is observed at T_r =0. Initially, the temperature deviation increases with the absolute value of T_r until a certain T_r value is reached, after which it gradually decreases with further increases in $|T_r|$.

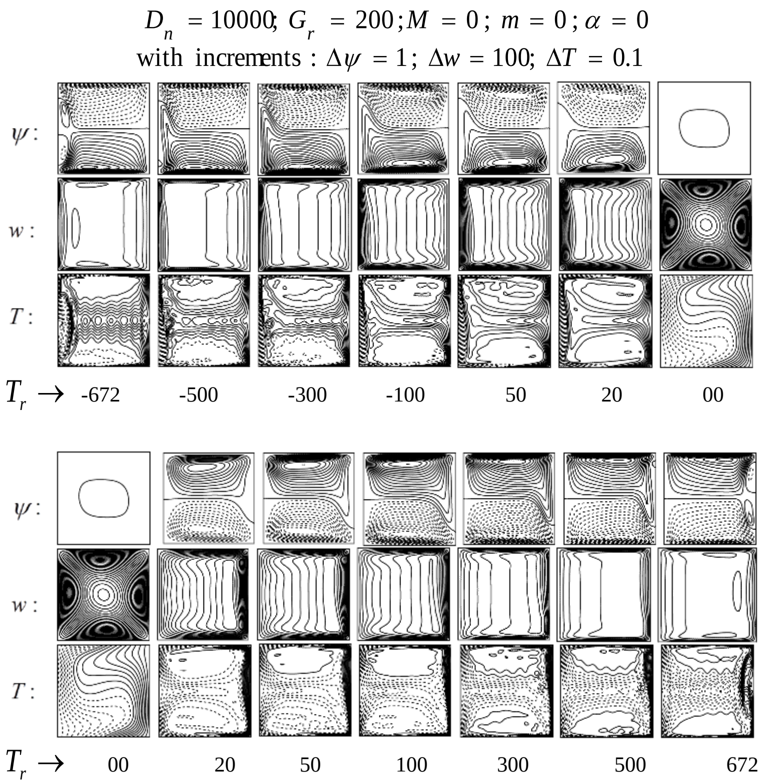

Figure 3*b*: Streamlines ψ (top), axial Contour flow w (middle) and Temperature profile T (bottom) in accordance with the solution curve in Fig.3*a*.

4.3 Effect of Dean Number (D_n) on the Fluid Velocity and Temperature

In Figure 4*a*, you can see the solution curve of Dean Number (D_n) versus (*i*) velocity flux and (*ii*) mean Nusselt number (*Nu*), which represents temperature variations, at the cooling and heating walls. These results are obtained with fixed values of G_r=200, T_r=20, P_r=7, M=0, m=0, and α=0. The solution curve is found for all positive values of the Dean Number. Three bifurcation solution curves are observed in a small range 25957.8 < D_n < 2722.7 (approximately). In all the solution curves, the flux increases with the increase of Dean Number. However, for the temperature, the values of the Nusselt number at the heating wall are higher than at the cooling wall, except at D_n =0. This difference gradually increases with the increase of D_n .

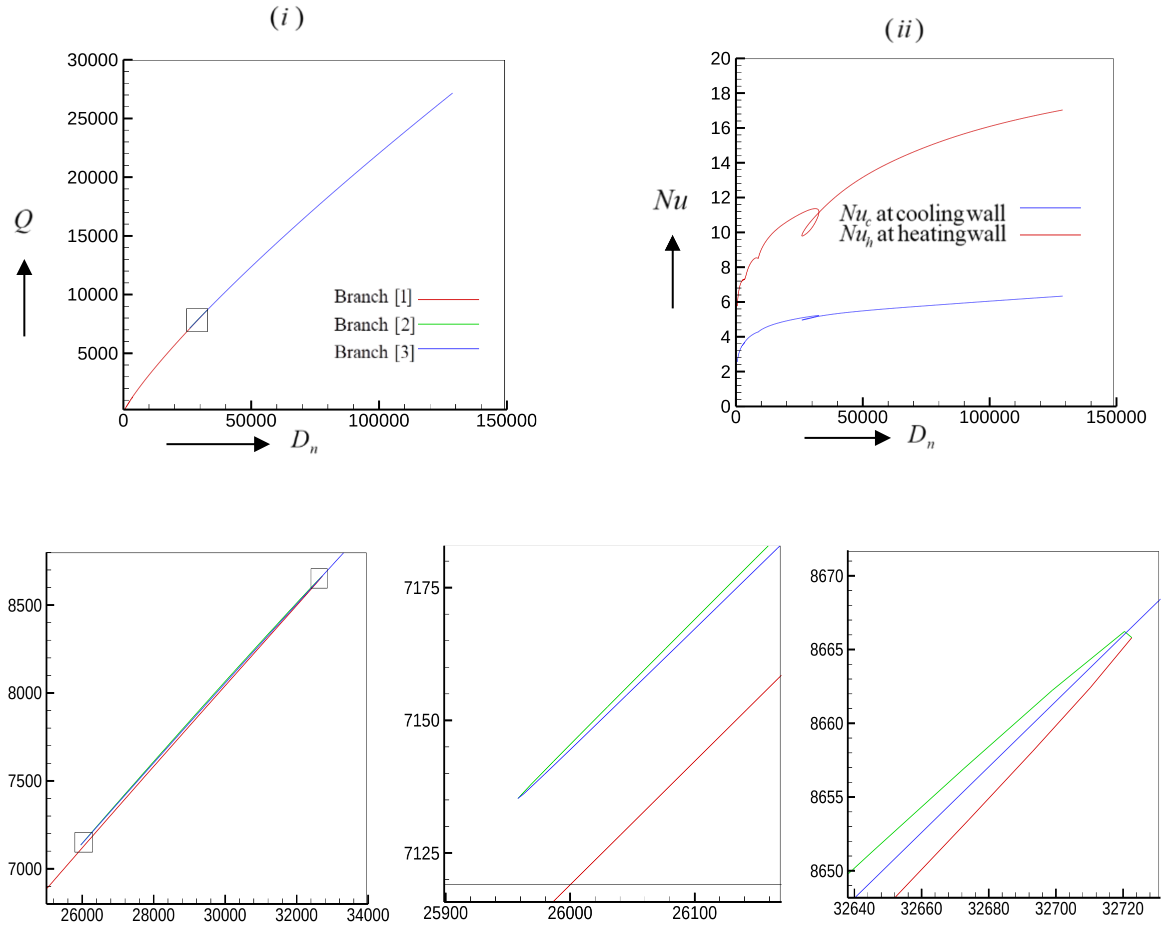

Figure 4*a*: Solution curve of D_n versus (*i*) flux Q (*ii*) Mean Nusselt number Nu at the heating and cooling wall for fixed T_r = 20, G_r = 200, P_r = 7, M = 0, m = 0 and α=0.

In Figure 4*b*, it is observed that the corresponding flow structures, including vortex structures of streamlines, contour distributions of axial flow, and temperature patterns. In all branches of the steady-state solution curve, a pair of counter-rotating vortices is observed for the secondary flow. The dominance between negative and positive rotational flow is reversed as D_n increases. The strength of the flow patterns gradually increases with the increase in D_n, both for velocity and temperature distribution. Asymmetrical flow structures are found in the 1st and 3rd branches of the steady-state solution curves. For the temperature distribution, the heated flow is dominated by the cooling flow.

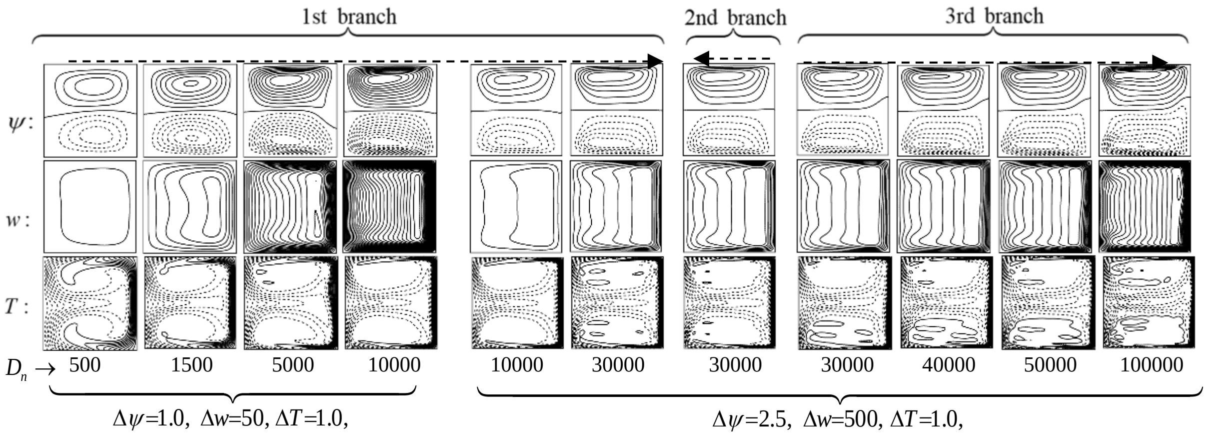

Figure 4*b*: Streamlines ψ (top), axial Contour flow w (middle) and Temperature profile T (bottom) in accordance with the solution curve in Fig.4a.

4.4 Effects of Magnetic Parameter (M) on the Fluid Velocity and Temperature

Figure 5*a* shows the solution curve representing the relationship between the Magnetic parameter (M) with (i) the velocity flux (Q) and (ii) the mean Nusselt number (Nu) for the cooling and heating walls in the context of temperature distribution. These findings are presented with consistent parameters, including G_r=200, T_r=20, P_r=7, m=0, and α=0. This investigation explores the influence of M across three different scenarios characterized by varying Dean Numbers such as D_n =500, 5000 and 10000.

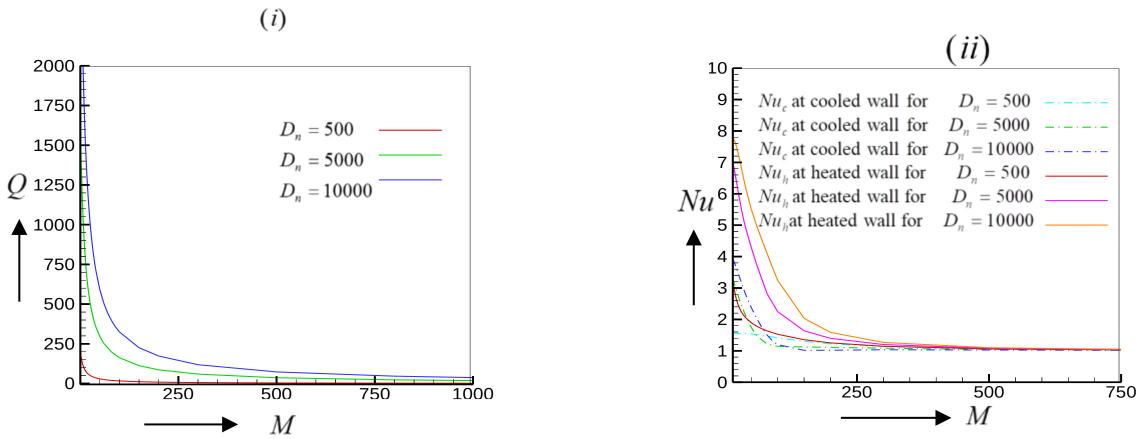

Figure 5*a*: Solution curve of M versus (i) flux Q (ii) Mean Nusselt number Nu at the heating and cooling wall for fixed T_r = 20, G_r = 200, P_r = 7, m = 0 and α=0 where D_n = 500,5000,10000.

In all scenarios, the solution curves exhibit a decreasing trend, leading to a reduction in flux as M increases. For high values of M, fluxes tend to approach zero. It's worth noting that the fluxes increase with higher Dean Numbers. Regarding temperature, the Nusselt numbers at the heating wall consistently surpass those at the cooling wall. The temperature deviation slowly approaches zero after a certain threshold value of M.

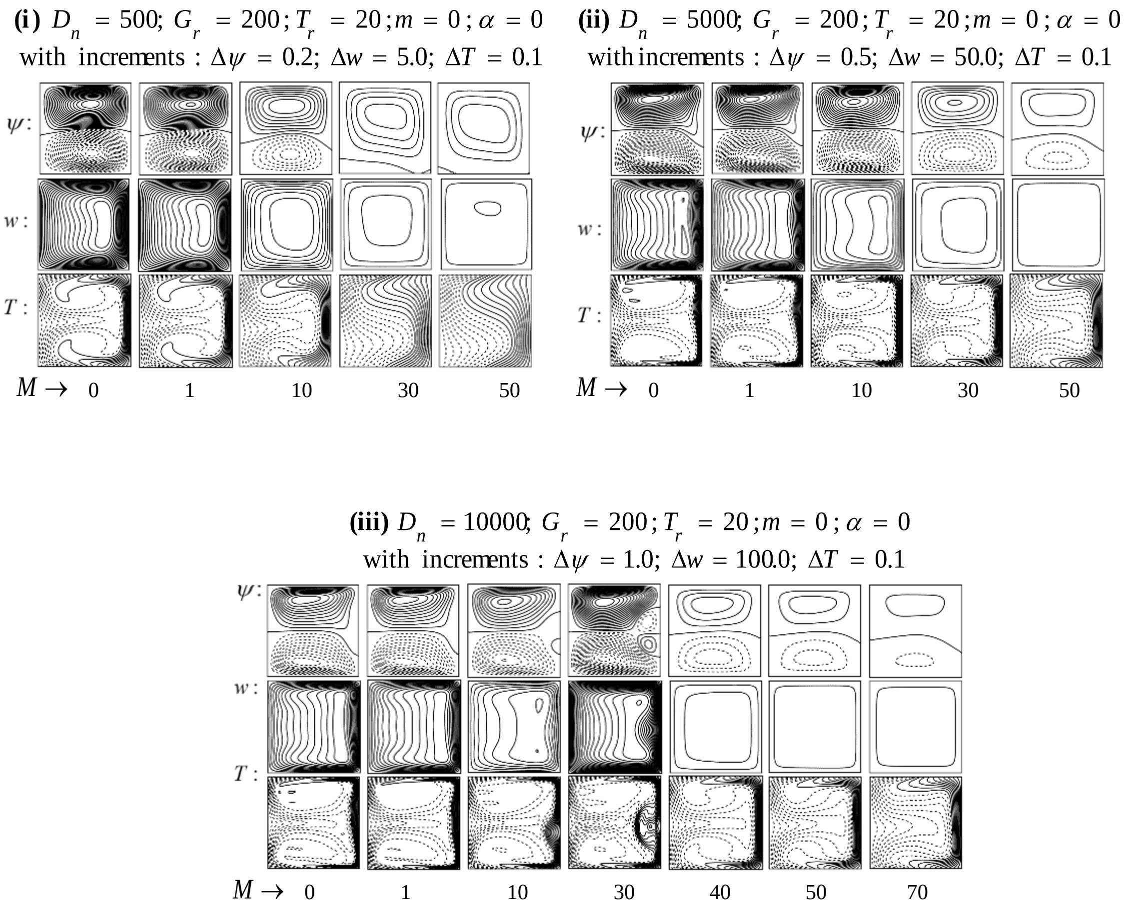

Figure 5*b*: Streamlines ψ (top), axial Contour flow w (middle) and Temperature profile T (bottom) in accordance with the solution curve in Fig.5*a*.

In Figure 5*b*, it has been seen the vortex structures, contour distributions for velocity, and patterns of temperature flow. As M becomes larger, the strength of velocity distribution gradually weakens. Concerning temperature, the cooling wall's temperature dominates over the heating wall's temperature, and this dominance effect diminishes as M increases across all the Dean Number.

4.5 Effects of Hall Parameter (m) on the Fluid Velocity and Temperature

Figure 6*a* presents the solution curve for the Hall parameter (m) versus (*i*) the flux (Q) for velocity and (*ii*) the mean Nusselt number (Nu) at the cooling and heating walls for temperature. The fixed parameters are G_r=200, T_r=20, P_r=7, M=13, and α=0 whereas three different Dean Numbers D_n = 500, 5000, and 10000 are considered. In all Dean Number scenarios, the solution curves exhibit an increasing trend for the Hall parameter (m). The flux increases rapidly with a growing m within a specific range, approximately $0 \le m \le 5$. After this initial rapid increase, it exhibits a minor increase and eventually reaches a steady-state solution beyond a certain threshold value of m.

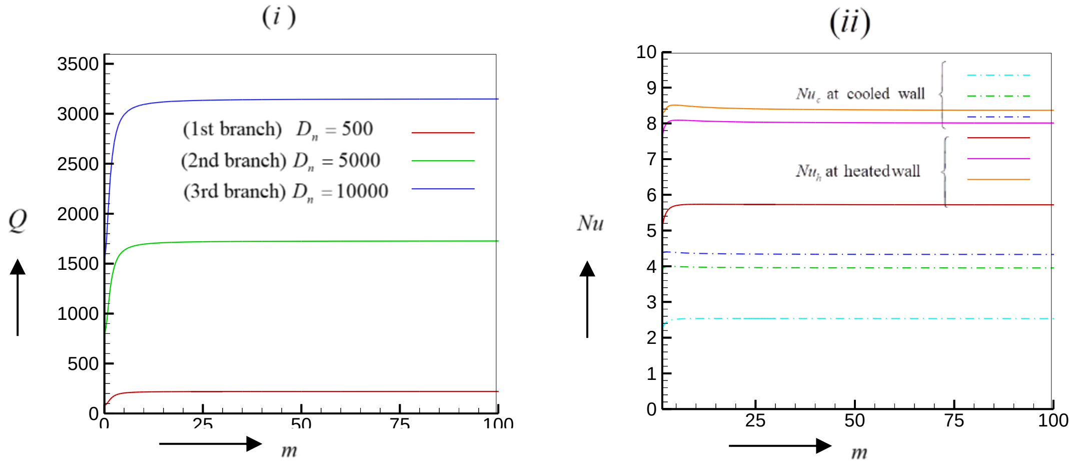

Figure 6*a*: Solution curve of m versus (*i*) flux Q (*ii*) Mean Nusselt number Nu at the heating and cooling wall for fixed $T_r = 20$, $G_r = 200$, $P_r = 7$, $M = 13$ and $\alpha = 0$ where $D_n = 500, 5000, 10000$.

The maximum flux is achieved at *m* values exceeding 200 (approximately). The numerical results show maximum flux values of 221, 1728.18, and 3150.84 for Dean Numbers 500, 5000, and 10000, respectively. It's worth noting that the flux increases with higher Dean Numbers. Regarding temperature, the Nusselt numbers at the heating wall consistently surpass those at the cooling wall across all *m* values. However, the temperature deviations remain unchanged as *m* increases.

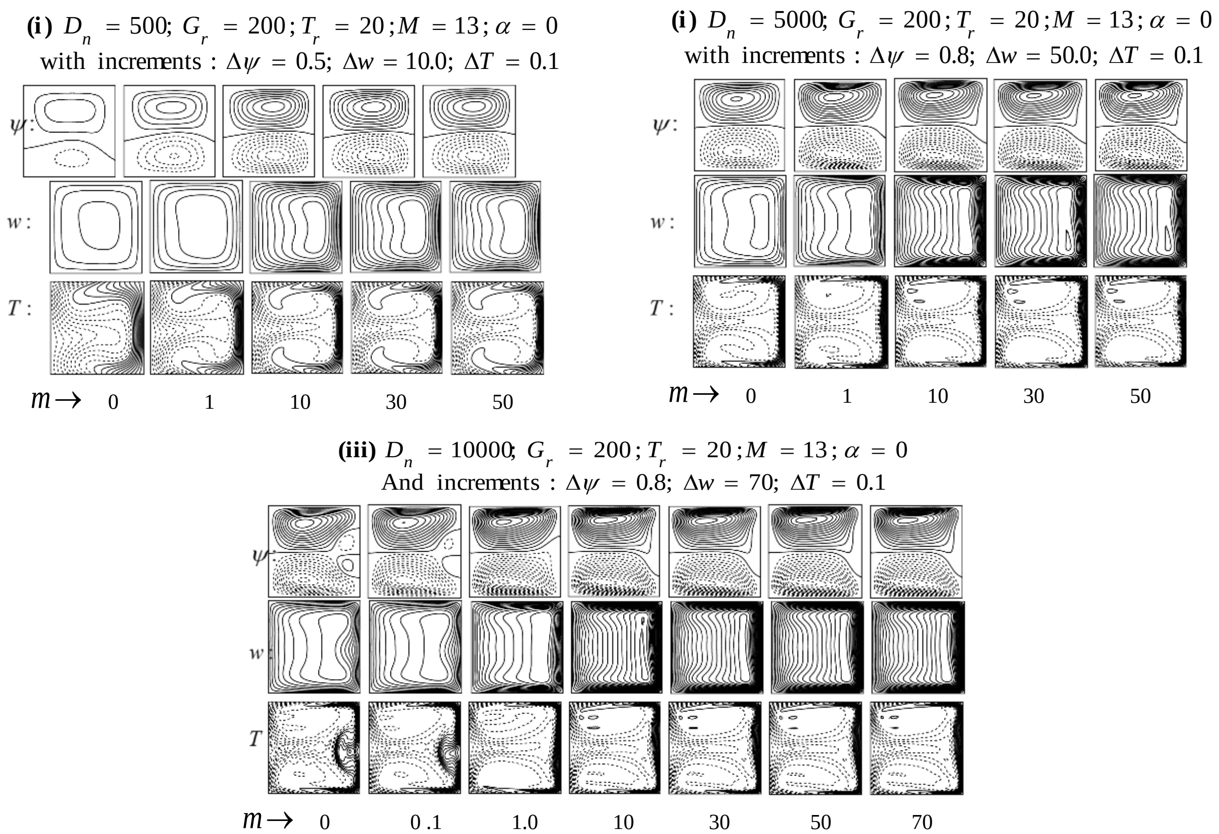

Figure 6*b*: Streamlines ψ (top), axial Contour flow w (middle) and Temperature profile T (bottom) in accordance with the solution curve in Fig.6*a*.

Figure 6*b* provides a visualization of the vortex structures, velocity distribution contours, and temperature flow patterns. These correspond to the solution curve depicted in Figure 6.7*a* at specific Hall parameter values. The strength of the velocity and temperature distribution exhibits an increase in pattern intensity within the range $0 \leq m \leq 10$. After this range, the structures remain consistent and do not change with further increases in *m*. Notably, for Dean Number D_n=10000, a pair of vortices is created in the secondary flow.

Regarding temperature, it's observed that the heating wall temperature consistently dominates over the cooling wall temperature across various m values. This effect remains unchanged with increasing m for all Dean Number scenarios.

4.6 Effects of Ion-slip Parameter (α) on the fluid flow and Temperature

Figure 7*a* presents the solution curve for the Ion-slip parameter (α) versus (*i*) the flux (Q) for velocity and (*ii*) the mean Nusselt number (Nu) at the cooling and heating walls for temperature. The fixed parameters are G_r=200, T_r=20, P_r=7, M=13, and m=0.1, whereas three different Dean Numbers D_n = 500, 5000, and 10000 are considered.

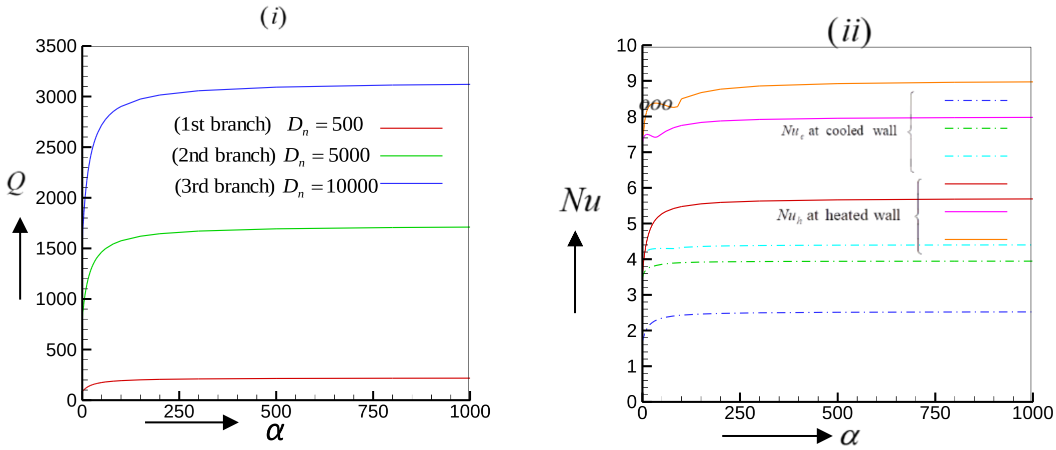

Figure 7*a*: Solution curve: Ion-slip parameter α versus (*i*) flux Q (*ii*) Mean Nusselt number Nu at the heating and cooling wall for fixed T_r = 20, G_r = 200, P_r = 7, M= 13 and m=0.1 where $D_n = 500, 5000, 10000$.

For all cases of Dean Number, the solution curves exhibit an increasing trend as the Ion-slip parameter (α) varies. There is a rapid increase in flux within a certain range, typically between $0 \leq \alpha \leq 200$, followed by a gradual increase in flux, and eventually, a steady-state solution is reached after a specific value of α. The maximum flux is achieved when α is greater than or equal to 750 (approximately). The numerical results show maximum flux values of 217.7, 1710.4, and 3134.8 for Dean Numbers D_n =500, 5000, and 10000 respectively. It is also confirmed that the flux increases with an increase in Dean Number. Concerning temperature, the Nusselt number values at the heating wall consistently exceed those at the cooling wall across various values of α. Importantly, the temperature deviation remains constant after reaching a certain value of α.

In Figure 7*b*, the vortex structures, velocity distribution contours, and temperature flow patterns corresponding to the solution curve of Figure 6.8*a* are presented at specific points along the Ion-slip parameter. Within the range of $0 \leq \alpha \leq 10$, both velocity and temperature distributions exhibit robust patterns. However, beyond this range, the structures remain relatively consistent and do not significantly change with further increases in α.

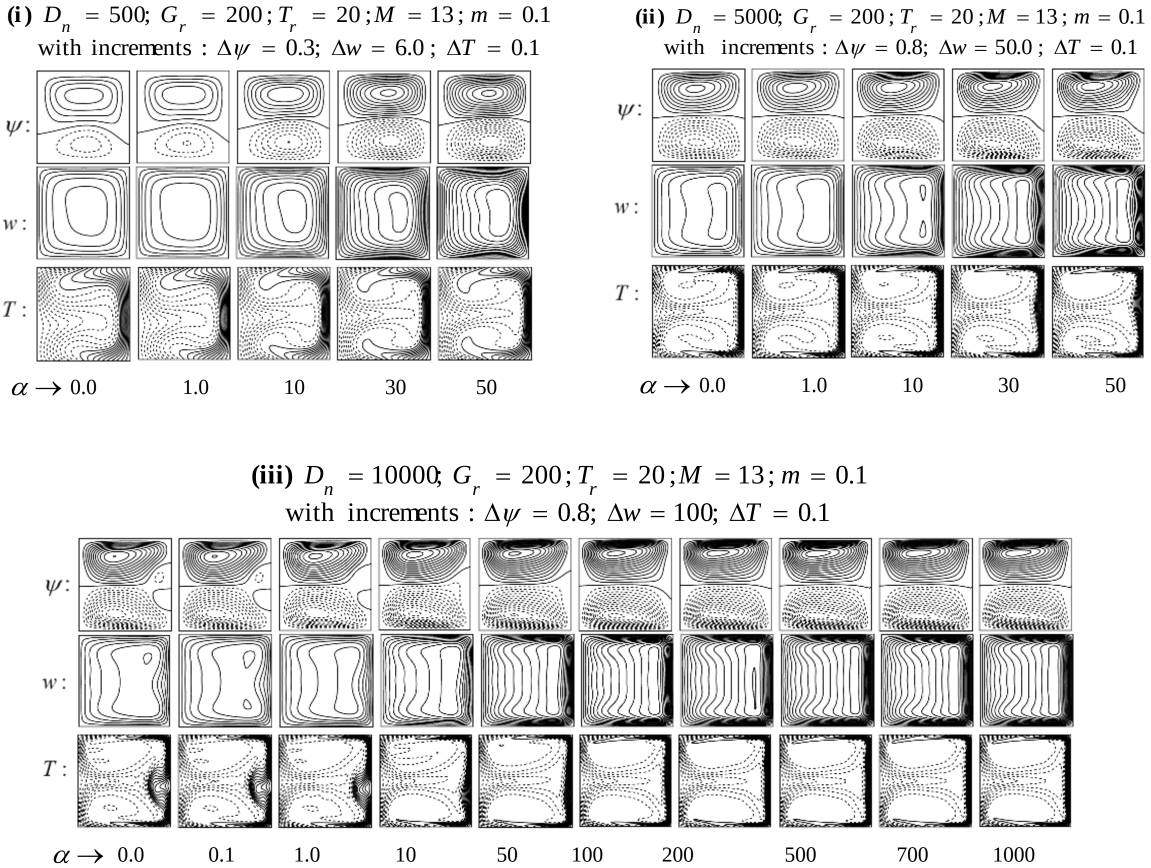

Figure 7*b*: Streamlines ψ (top), axial Contour flow w (middle) and Temperature profile T (bottom) in accordance with the solution curve in Fig.7*a*.

Notably, in the case of Dean Number $D_n = 10000$, a pair of vortices emerges in the secondary flow. Additionally, in terms of temperature, the heating wall temperature consistently dominates the cooling wall temperature throughout the evaluated range of Ion-slip parameter (α).

Conclusions

The present numerical results are accurately and sufficiently compared to the previously published experimental results. Therefore, it is conceivable that the study's findings are valid. The findings, which are based on the thorough examination of the relevant parameters discussed above, can be summarized as follows:

***Velocity Profile*:**

1. The solution curves exhibit an increasing trend for parameters like G_r ($G_r > 0$), T_r ($T_r < 0$), D_n ($D_n > 0$), m ($m > 0$), and α ($\alpha > 0$). Consequently, the flux increases within these parameter ranges.
2. Conversely, the solution curves demonstrate a decreasing trend for parameters like G_r ($G_r < 0$), T_r ($T_r > 0$), and M ($M > 0$). Consequently, the flux decreases within these parameter ranges.
3. The fluid velocity structure is initially symmetric at $G_r = 0$, but this symmetry gradually becomes asymmetric as $|G_r|$ increases.
4. The solution curve remains symmetric about the vertical line at $T_r = 0$.
5. Steady-state solution branches exhibit a pair of counter-rotating vortices for the secondary flow in all cases.

6. The fluid velocity's strength increases with higher values of D_n and T_r, while it weakens with higher values of M.
7. The strength of both velocity and temperature distributions becomes strong within a certain parameter range, and beyond this range, their structures remain unchanged with increasing values of m and α.

***Temperature Profile*:**

1. At various parameter variations, including G_r, T_r, D_n, M, m, and α, the Nusselt number values at the heating wall are consistently higher than those at the cooling wall.
2. The heating flow consistently dominates over the cooling flow across different parameter variations, including G_r, T_r, D_n, M, m, and α.
3. No temperature deviation is observed at $T_r = 0$. The temperature deviation gradually increases with the absolute value of T_r until a certain T_r value, after which it decreases slowly as the absolute value of T_r continues to rise.
4. The temperature deviation gradually increases with the increase in D_n.
5. The temperature deviation decreases as M increases.
6. The temperature deviation remains constant beyond certain values of m and α.

Incorporating Hall and Ion-slip currents in the study of straight duct flow has considerable significance not only in improving the efficiency of mechanical devices but also in advancing our understanding of fluid dynamics in various engineering applications. Given that the universe consists of highly charged particles and is influenced by magnetic fields, these considerations provide a more accurate framework for analyzing the behaviour of fluid flow in the ducts. Based on the insights discussed above, the utilization of Hall current and Ion-slip in the context of straight duct flow represents a promising and valuable avenue for research in the field of magneto-hydrodynamics (MHD) and engineering applications.

References

Berger S. A., Talbot L and Yao L.S. Flow in curved pipes. *Ann. Rev. Fluid Mech.* 1983; Vol.15, pp 461- 512.

Chandratilleke T.T., Nadim N. And Narayanaswamy R. Analysis of secondary flow instability and forced convection in fluid flow through rectangular and elliptical curved ducts. Heat Transf. Eng. 2013; 34, 1237–1248. https://doi.org/10.1080/01457632.2013.777249.

Chandratilleke T.T., Nursubyakto. Numerical prediction of secondary flow and convective heat transfer in externally heated curved rectangular ducts. *Int. J. Therm. Sci*. 2003; **42**, 187–198. https://doi.org/10.1016/S1290-0729(02)00018-2.

Chandratilleke, T.T, Nadim, N. and Narayanaswamy, R. Vortex structure-based analysis of laminar flow behavior and thermal characteristics in curved ducts. Int.J. Thermal Sci. 2012; 59: 75-86. https://doi.org/10.1016/j.ijthermalsci.2012.04.014.

Dean, W.R. Note on the motion of fluid in a curved pipe. *Philosophical Magazine and Journal of Science,* 1927; Vol. 4: Issue 20, pp 208-23. http://dx.doi.org/10.1080/14786440708564324.

Dean, W.R. Note on the Motion of Fluid in a Curved Pipe. *Philosophical Magazine and Journal of Science,* 1928; Vol. 5: Issue 30, pp 673-695. http://dx.doi.org/10.1080/14786440408564513.

Fellouah, H., Castelain, C., Ould-ElMoctar, A. and Peerhossaini, H. The Dean Instability in Power-law and Bingham Fluids in a Curved Rectangular Duct. *Journal of NonNewtonian Fluid Mech*. 2010; Vol. 165, pp. 163–173.

Gottlieb, D. and Orszag, S. A. Numerical Analysis of Spectral Methods, Society for Industrial and Applied Mathematics." *Philadelphia, USA,* 1977; https://doi.org/10.1137/1.9781611970425.

Ishigaki H. Laminar Flow in Rotating Curved Pipes. *Journal of Fluid Mechanics*, 1996; 329, pp. 373-388. https://doi.org/10.1017/S0022112096008956.

Kun, M. A, Yuan S., Chang, H. and Lai, H. Experimental Study of Pseudoplastic Fluid Flows in a Square Duct of Strong Curvature. *J. Thermal Science* 2014; Vol. 23, No. 4, pp. 359−367.

Li, Y., Wang, X., Yuan, S., Tan, S.K. Flow development in curved rectangular ducts with continuously varying curvature. *Experimental Thermal and Fluid Science,* 2016; 75: 1-15.

Li, Y., Wang, X., Zhou, B., Yuan, S., Tan, S.K. Dean instability and secondary flow structure in curved rectangular ducts. *Int. J. Heat and Fluid Flow*, 2017; 68: 189-202. https://doi.org/10.1016/j.expthermflusci.2016.01.012.

Liu, F. and Wang, L. Analysis on multiplicity and stability of convective heat transfer in tightly curved rectangular ducts. *Int. J. Heat and Mass Transfer*, 2009; 52: 5849-5866.

Nandakumar, K and Masliyah J.H. Swirling flow and heat transfer in coiled and twisted pipes. *Adv. Transport. Process.* 1986; 4, 49-112.

Nandakumar, K. and J.H. Masliyah. Bifurcation in steady laminar flow through curved tubes. *J. Fluid Mech*. 1982; 119, pp. 475-490.

Norouzi, M., Kayhani, M.H., Nobari, M.R.H. and Demneh, M.K. Convective heat transfer of viscoelastic flow in a curved duct. *World Acad. Sci. Eng. Tech*. 2009; 32:327-33.

Razavi, S.E., Soltanipour, H., Choupani, P. Second law analysis of laminar forced convection in a rotating curved duct. *Thermal Sciences*, 2015; 19(1): 95-107. https://doi.org/10.2298/TSCI120606034R.

Selmi, M. and Namdakumar, K. and Finlay W.H. A Bifurcation Study of Viscous Flow Through a Rotating Curved Duct. *J. Fluid Mechanics*, 1994; 262, pp. 353-375.

Selmi, M. and Nandakumar, K. Finlay "Bifurcation study of flow through rotating curved ducts. *Phys. Of Fluids,* 1999; 11, pp 2030-2043.

Wang, L. and Yang, T. Bifurcation and Stability of Forced Convection in Rotating Curved Ducts of Square Cross Section. *Int. J. Heat Mass Transfer*, 2003; Vol. 46, pp.613-629.

Wang, L.Q. and Liu F. Forced Convection in Tightly Coiled Ducts: Bifurcation in a High Dean Number Region. *International Journal of Non-Linear Mechanics*, 2007; 42, pp. 1018-1034.

Wang, L.Q. and Liu, F. Forced Convection in Slightly Curved Microchannels. *Int. J. Heat Mass Transfer*, 2007; 50, pp. 881-896.

Wang, L.Q. and Yang, T.L. Multiplicity and Stability of Convection in Curved Ducts: Review and Progress. *Adv. Heat Transfer*, 2004; 38, pp. 203-256.

Winters, K.H. A bifurcation Study of Laminar Flow in a Curved Tube of Rectangular Cross-section. *Journal of Fluid Mechanics*, 1987; 180, pp.343-369.

Wu, X.Y., Lai, S.D., Yamamoto, K. and Yanase, S. Numerical analysis of the flow in a curved duct. *Advanced Materials Research*, 2013; 706-708: 1450-1453. https://doi.org/10.4028/www.scientific.net/AMR.706-708.1450.

Yamamoto, K., Alam, M. M., Yasuhara, J. and Aribowo, A. Flow through a rotating helical pipe with circular cross section. *J. Heat and fluid flow*, 2000; 21, pp213-220.

Yamamoto, K., Xiaoyum, W., Kazou, N., Yasutuka, H. Visualization of Taylor-Dean flow in a curved duct of square cross section. *J. Fluid Dyn. Res.* 2006; 38: 1-18.

Yamamoto, K., Yanase, S. and Alam, M.M. Flow Through a Rotating Curved Duct withSquare Cross-section. *J. Phys. Soc. Japan*, 1999; 68, pp. 1173-1184.

Yanase, S. Kaga, Y. and Daikai, R. Laminar flows through a curved rectangular duct over a wide range of the aspect ratio. *Fluid Dyn. Res*., 2002; 31 pp. 151-183. https://doi.org/10.1016/S0169-5983(02)00103-X.

Yanase, S. Goto, N. and Yamamoto, K. Dual solutions of the flow through a curved tube", *Fluid Dynamics Research*, 1989, Volume 5, Issue 3, December, pp. 191-201. https://doi.org/10.1016/0169-5983(89)90021-X.

Yanase, S., Watanabe, T. and Hyakutake, T. Traveling-wave solutions of the flow in a curved-square duct. *Physics of Fluids*. 2008; 20 (124101): 1-8. https://doi.org/10.1063/1.3029703.

Zhang, J.S., Zhang, B.Z., Jii, J. Fluid Flow in a Rotating Curved Rectangular Duct. *Int. J. Heat and Fluid Flow*, 2001 22, pp. 583-592.